Response to Reviewer #2 (Alexei Korolev)

Overall Recommendation

The airborne observations presented in this manuscript are potentially valuable and may provide useful evidence of enhanced ice concentrations consistent with secondary ice production in convective clouds over the Tibetan Plateau. However, the manuscript currently overinterprets the observations and attributes enhanced ice concentrations to specific SIP mechanisms without sufficient supporting evidence.

The most significant issues are:

- the unsupported identification of HM, DS, and BR mechanisms;
- the neglect of vertical transport as an alternative explanation for enhanced ice concentrations at cold temperatures;
- the uncertain identification of drizzle and large liquid drops;
- the overstated novelty of the IMF (SIP ratio), which is essentially equivalent to the Ice Multiplication Factor introduced by Wieder et al. (2022);
- the limitations of the IMF methodology when applied using parameterized rather than directly measured INP concentrations;
- the potential mathematical self-correlation in Figure 16.

A publishable paper could emerge from this study if the authors focus on robust observational evidence for enhanced ice concentrations and substantially reduce unsupported claims regarding the identification and relative importance of specific SIP mechanisms.

Reply:

We thank the reviewer for the detailed identification of the weaknesses of the previous version and for the constructive comments. We accept the central criticism: the earlier manuscript attributed enhanced ice concentrations to specific SIP mechanisms (HM, DS, BR) on the basis of local, Eulerian measurements, which cannot support such attribution. The objective of the paper has therefore been changed rather than merely softened. The study now aims to show the observational signatures of ice enhancement consistent with SIP in convective clouds over the TP, to examine how these signatures vary with temperature and with the concentrations of hydrometeors that can act as SIP partners, and to state explicitly what the dataset can and cannot resolve. Mechanism names are retained only as descriptions of particle assemblages ("consistent with"), and the alternatives of vertical transport and of several possible coexisting mechanisms are stated wherever cold-level enhancement is discussed.

The manuscript has been revised mainly as follows:

(1) The meteorological context has been expanded. Fig. 2 now includes distributions of the FY-2D visible image, brightness temperature (TBB), ground-based radar reflectivity and the Naqu sounding profile (wind, temperature, 0°C level, LCL, CCL).

(2) The round (drizzle) concentration has been recalculated from $0.9 \leq C < 1.2$ and D

≥ 90 μm, following the 50-pixel shape threshold of Taylor et al. (2016), and all figures and statistics involving round particles have been redrawn.

(3) The term "SIP ratio" has been removed. The metric is now the IMF=N_{ice}/N_{INP}, attributed explicitly to Field et al. (2017) and Wieder et al. (2022), with Nice restricted to irregular particles ($N_{ice}=N_{irreg}$). The uncertainty of the parameterized INP concentration and the limitations of the IMF methodology have been now discussed in Sect. 4.2.

(4) ERA5 vertical velocity fields (Horizontal distribution and vertical cross-section, Fig. 15) have been added, and the upward transport of secondary ice is now discussed as an alternative explanation that the data cannot exclude. In addition, a habit census by temperature bin in case 4 has been added (Fig. 13i).

(5) HVPS spectra have been added to Figs. 10 and 14, so that the ice, drizzle and large-particle spectra are now presented over the full 2DS10 to HVPS range.

(6) We have redrawn Figure 16 to discuss the relationship between ice concentration enhancement and the concentrations of drizzle (D ≥ 90 μm) and large hydrometeors (HVPS, D ≥ 300 μm) across different temperature intervals.

(7) Table 3 and Sect. 4.1 have been substantially expanded, covering the Northern Hemisphere, the Southern Hemisphere and the tropics.

We believe the revised manuscript is a more defensible contribution: it documents the ice enhancement, its temperature range, its spectral signature and its association with large droplets and hydrometeors.

Major Comments

1. Identification of specific SIP mechanisms is not supported by the observations

A major portion of the manuscript is devoted to distinguishing among HM, DS, and BR mechanisms using associations between elevated ice concentrations and four environmental parameters: temperature, droplet concentration, droplet size, and graupel occurrence.

A fundamental limitation of this approach is that no attempt is made to determine the age of sampled ice particles. As discussed by Korolev et al. (2020), secondary ice particles may be transported substantial distances from their source regions and lose their spatial correlation with the environmental conditions under which they formed. Consequently, the local environment at the aircraft sampling location may not represent the environment where SIP actually occurred.

This limitation is inherent to Eulerian airborne sampling and affects most in situ studies of SIP. Airborne measurements can reliably identify enhanced ice concentrations that may be interpreted as evidence of SIP. However, direct observation of the SIP process itself is generally not possible from aircraft moving at speeds of 100 m s−1 or greater.

Therefore, attributing enhanced ice concentrations to specific SIP mechanisms on the basis of local measurements of graupel, droplet size, droplet concentration, and temperature is not justified. I strongly recommend removing, or substantially reducing,

the discussion of SIP type throughout the manuscript and focusing instead on observational evidence of enhanced ice concentrations.

Reply:

We agree with this diagnosis and have restructured the manuscript rather than reworded it. The comment identifies two distinct problems, which we address separately: attribution to a specific mechanism cannot be established from Eulerian sampling, and the previous version nevertheless used local associations to rank mechanisms. Both have been corrected. Following the reviewer's comments, we have substantially reduced the discussion of SIP type throughout the manuscript and focusing instead on observational evidence of enhanced ice concentrations.

Claims attributing the ice enhancement to DS or BR have been weakened. Neither mechanism is now assigned a role in the observed enhancement, and the text no longer ranks the mechanisms or states that any one of them dominated. This does not mean that their contribution is excluded: the observations cannot resolve whether DS or BR also contributed, and the manuscript states this explicitly in Sects. 3.2.2 and 4.2.

In addition, we also discussed the possibility that the vertical transport of ice crystals contributes to the enhanced ice concentrations; the details will be addressed in our response to comment 2 below.

2. Enhanced ice concentrations observed below −8°C do not demonstrate active SIP at those temperatures

One of the central conclusions of the manuscript is that SIP remains active over a broad temperature range extending from approximately −3°C to −16°C and that multiple SIP mechanisms operate throughout this range.

However, the manuscript appears to assume that enhanced ice concentrations observed at colder temperatures were generated locally. This interpretation is not unique and may not be the most likely explanation.

An alternative explanation is that large concentrations of secondary ice particles formed at warmer cloud levels were subsequently transported upward by convective updrafts. Such vertical transport can readily produce enhanced ice concentrations at temperatures below −8°C without requiring active local SIP at those temperatures.

Korolev et al. (2020, 2024) discussed this issue extensively and demonstrated that enhanced concentrations of secondary ice particles can extend from regions immediately above the melting layer to substantially colder cloud levels. The presence of enhanced ice concentrations at cold temperatures does not necessarily imply that SIP was initiated there. Rather, these particles may simply have been transported from warmer levels where SIP was active. The central conclusion of that study was that airborne observations can only identify active SIP when very young ice particles are observed and cannot reliably infer SIP source regions from aged ice populations alone.

The present study does not distinguish between: (a) local SIP occurring at temperatures T< −8°C, and (2) secondary ice produced at warmer temperatures and transported upward. The available observations do not appear capable of separating these two scenarios. Therefore, the statement that SIP is active throughout the entire temperature range down to −16°C is not supported by the presented evidence.

The observations demonstrate that enhanced ice concentrations were observed

down to −16°C. They do not demonstrate that secondary ice production was actively occurring throughout this temperature range.

Reply:

For the ice enhancement at −8 °C, we fully agree with the reviewer's reasonable explanation that secondary ice crystals formed in the warm layer were transported vertically to the cold layer. We statistically analyzed the proportions of ice crystal habits within different temperature ranges in case 4 (Fig. 13i) and found that columnar ice crystals in the layer warmer than −8 °C were nearly twice as abundant as those in the cold layer. Therefore, columnar ice crystals do not dominate in the cold layer. We suggest that these columnar ice crystals were mainly secondary ice generated in the warm layer and carried to the cold layer by updrafts (based on ERA5, Fig. 15), thereby causing the ice enhancement. Of course, other local SIP processes may also occur in the cold layer. However, with the current data, it is very difficult to separate these two processes. A detailed analysis has now been added in Sect. 3.2.2 of the manuscript (Lines 396-427):

Finally, one question remains unresolved: where did the columnar crystals detected at the cold levels come from? According to the habit diagram of Bailey and Hallett (2009), columnar habits form mainly at temperatures warmer than about –10°C, so their presence at 8–8.6 km (down to –16°C) is not readily explained by primary growth at those temperatures and instead points to a source region at warmer levels. Secondary production of columnar crystals at these temperatures is no more plausible than primary growth, because columnar crystals are the characteristic product of HM and splintering is efficient only within the –3 to –8°C window (Hallett and Mossop, 1974). Griggs and Choularton (1983) further suggested that rimed droplets freeze so rapidly below –8°C that the resulting ice shell becomes too rigid to splinter. Taylor et al. (2016) offered a transport-based explanation for their presence at cold levels: although columnar crystals are an expected product of HM splintering mainly within the –3 to –8°C range, they can also be observed at other temperatures when displaced by updrafts and downdrafts. Their occurrence at cold levels therefore may point to vertical transport from the warm layer. Moreover, the column class was about twice as abundant in the warmer bins (about 6.5–7.8%) as in the colder bins (about 3.4–4.3%), consistent with preferential production in the warm HM layer and subsequent transport to the cold levels. The ERA5 vertical-velocity fields in Fig. 15 provide a first-order test of this transport pathway. In the horizontal distributions, broad regions of upward motion were present over and around the case 4 domain at 450, 400 and 350 hPa (about 6.6, 7.5 and 8.5 km; Figs. 15a–f), and the updraft signal extended up to 350 hPa. The vertical cross-sections along 31.75°N (Figs. 15g and 15h) show coherent upward motion across the 6–9 km layer, linking the warm HM layer near 6.3 km to the cold sampling height near 8.6 km. This upward motion was more pronounced at 11:00 than at 10:00, with 11:00 being the case 4 sampling time. Such sustained updrafts offered a natural pathway for lofting columnar crystals from lower (warmer) levels to the cold levels below –10°C, a process that Korolev et al. (2020, 2024) showed can supply secondary ice to substantially colder cloud layers. The columnar crystals at cold levels are therefore better explained by upward transport from the warmer HM layers than by

local formation, although a minor locally produced contribution cannot be excluded from the crystal habits alone.

The observations presented here also shed light on the cold-level ice enhancement in case 4. Primary nucleation alone cannot account for it, since the ice concentrations at these levels exceeded the N_{INP} by two to three orders (−8 to −13°C) and by one to two orders near −16°C (Fig. 12). A plausible supply is the upward transport of secondary ice from the warmer HM layers, which would by itself raise the ice concentration at cold levels (Korolev et al., 2020, 2024). In-situ SIP within the cold layer, however, may contribute as well, since supercooled large droplets and large hydrometeors persisted below –10°C (Figs. 11 and 14), providing conditions favorable for SIP. Part of the needle class may consist of fine fragments produced locally by BR. The particle populations required by such pathways were likewise present in the cold layer: graupel remained the most abundant large hydrometeor below –13°C (about 9%, Fig. 13i), and dendritic crystals, although few in number, were still present, so the dense and the fragile particle types whose collisions are invoked in the BR process were both available. The drizzle that persisted below –10°C likewise provided the supercooled large droplets required by droplet-shattering pathways. However, we cannot quantify the vertical transported versus locally secondary ice formed fractions based on present dataset.

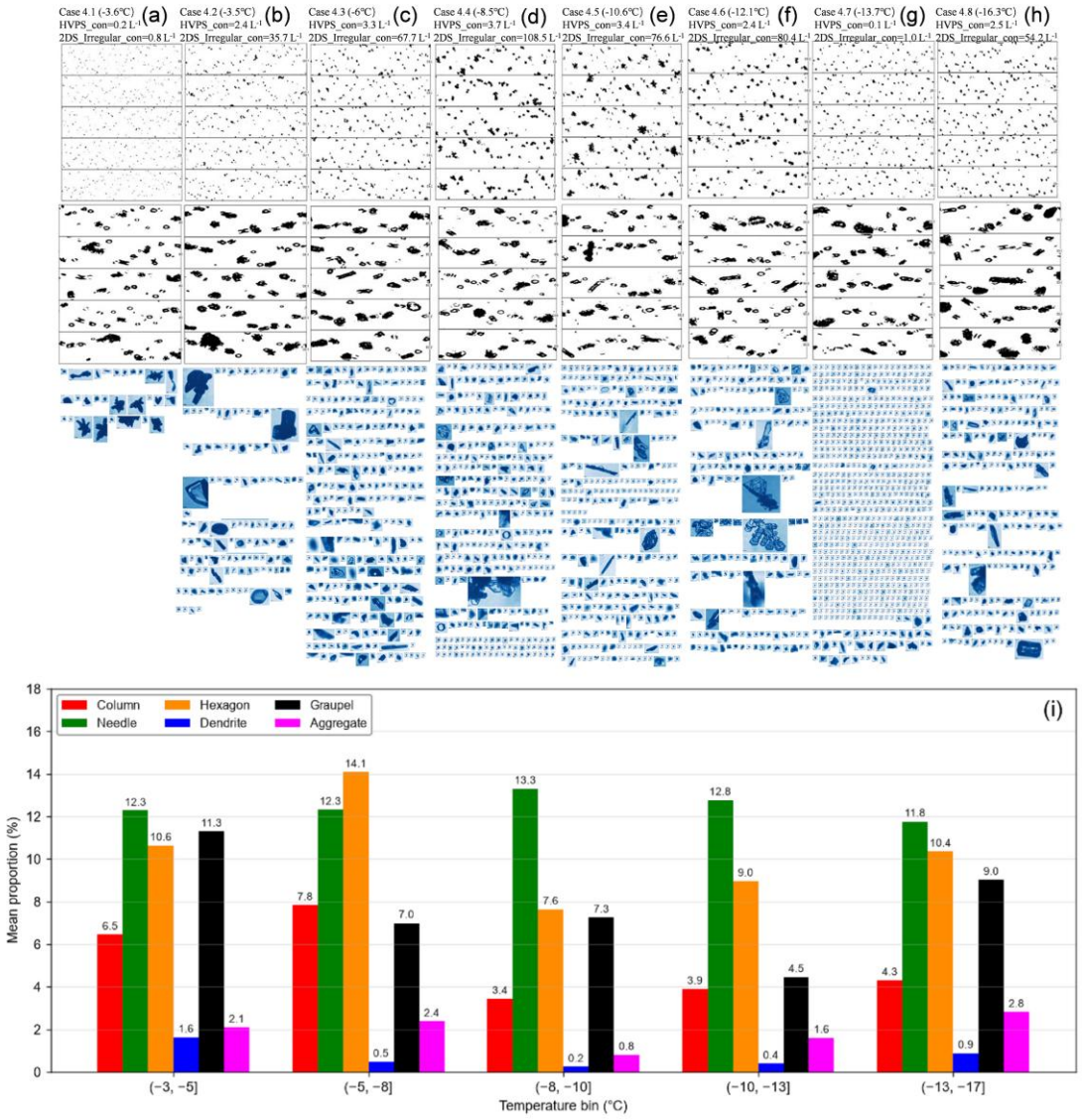

Figure 13: Example images (a–h) of 2DS and CPI from −3.6 to −16.3℃ in case 4; values at the top of each image indicate average temperature and particle concentration. (i) Mean relative abundances of six ice crystal habit classes as a function of temperature in case 4, binned into intervals of (−3, −5], (−5, −8], (−8, −10], (−10, −13], (−13, −17] ℃. Habits were classified from 2DS10 images into eight classes; the six ice habits (column, needle, dendrite, hexagon, aggregate and graupel) are shown, whereas broken and spherical particles are omitted, so the six series do not sum to 100%.

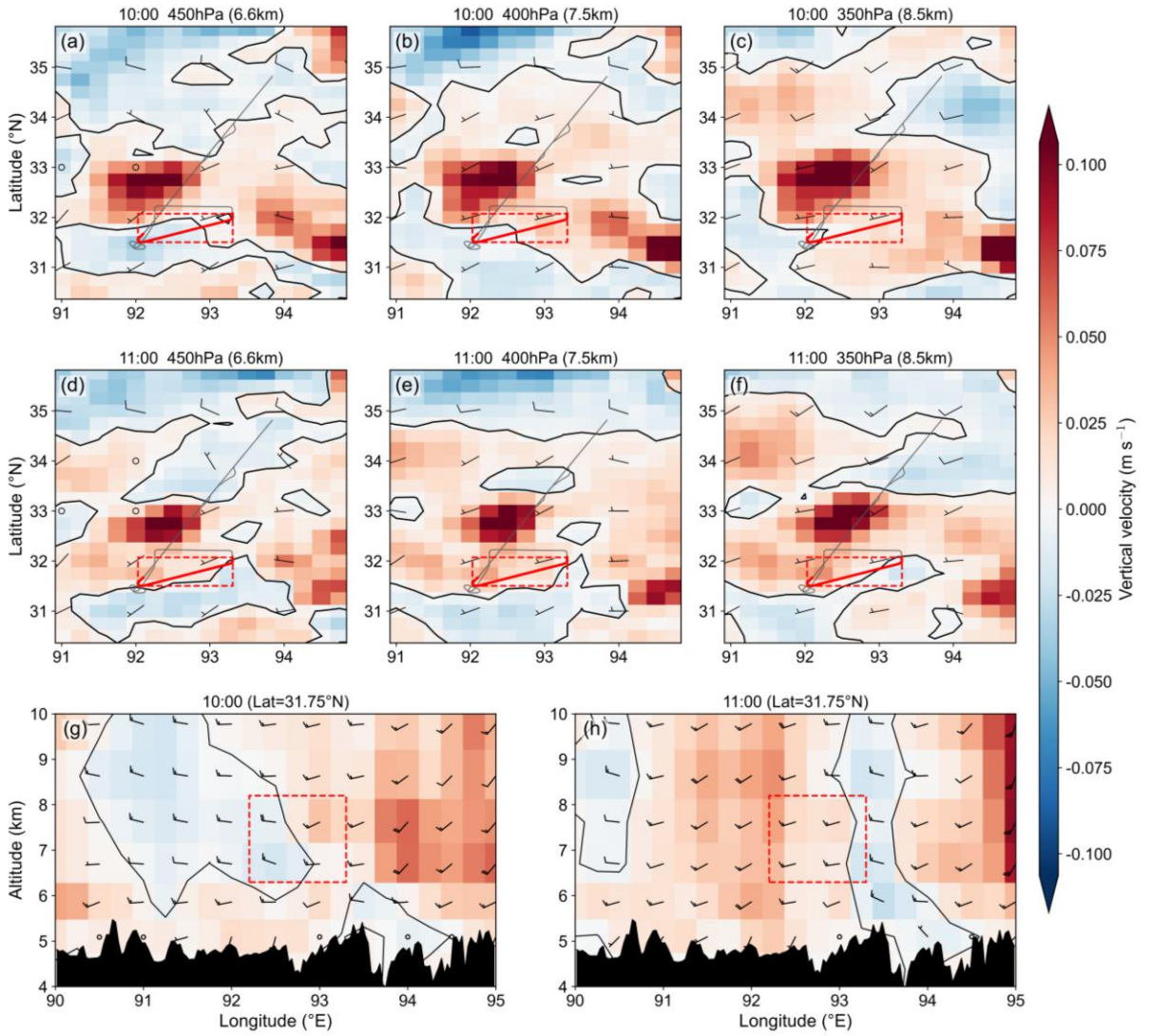

Figure 15. ERA5 vertical velocity (m s^{-1}, upward positive) over the flight region on 6 July 2014: horizontal distributions at 450/400/350 hPa for 10:00 (a–c) and 11:00 (d–f), and vertical cross-sections along 31.75°N for 10:00 (g) and 11:00 (h). Black contours are w = 0; barbs show horizontal wind (cross-sections: u and w×100). Gray/red lines are the full track and case 4 segment (11:15–11:40); red dashed boxes mark the case 4.

3. The introduction of the SIP ratio is overstated and its limitations require greater discussion

The manuscript introduces the quantity

$$SIP\ ratio = \frac{N_{ice}}{N_{INP}}$$

as a primary metric for characterizing SIP.

The presentation of this metric creates the impression that it represents a new approach. However, this is not the case.

Comparison of ice particle concentration (N_{ice}) with ice-nucleating particle concentration (N_{INP}) has been used for decades as a basic approach for identifying secondary ice production (Field et al., 2017). More recently, Wieder et al. (2022) formalized this ratio as the Ice Multiplication Factor (IMF). Since then, the cloud physics community has used the IMF to characterize SIP events in remote sensing and

in situ observations.

Therefore, the "SIP ratio" introduced here is not a new metric but effectively equivalent to the IMF described by Wieder et al. (2022). The manuscript should avoid presenting the SIP ratio as a novel contribution. There is also no need to rename the conventional names established in the cloud physics community. For consistency I will keep using the conventional IMF abbreviation instead of SIP ratio in the rest of my review.

The interpretation of this quantity also requires greater caution. In this study, N_{INP} is not measured directly but estimated using the DeMott et al. (2010) parameterization. Such estimates are subject to potentially large uncertainties because primary nucleation may occur on INPs transported by convective updrafts or entrained from above cloud top, whereas aerosol measurements and parameterizations may not accurately represent the INP population responsible for primary ice formation.

Another concern is that Figure 16 includes many observations with IFM values substantially below one. Assuming that N_{ice} and N_{INP} characterize the same cloud volume, one would generally expect $N_{ice}/N_{INP} \geq 1$, because each activated INP can generate at most a primary ice particle before SIP occurs. The occurrence of numerous cases with $N_{ice}/N_{INP} \ll 1$ raises questions about the representativeness of the estimated INP concentrations and emphasizes limitations of the IMF methodology in the present study.

The uncertainty of the INP estimates should be quantified and discussed in much greater detail.

Reply:

(1) The definition of IMF

We have removed the SIP ratio, and the manuscript now consistently uses IMF to quantify ice enhancement (Sect. 2.3, IMF=N_{ice}/N_{INP}). Here, N_{ice} is the concentrations of irregular particles (ice) from the 2DS10 and does not include the round (D ≥ 90 μm) concentrations. N_{INP} values were estimated using the parameterization of DeMott et al. (2010).

(2) Discussion of INP uncertainty

We have re-estimated the INP concentrations, as shown in Fig. 5c. Between −2 and −20°C, the INP concentrations were below or near to 1 L^{-1}.

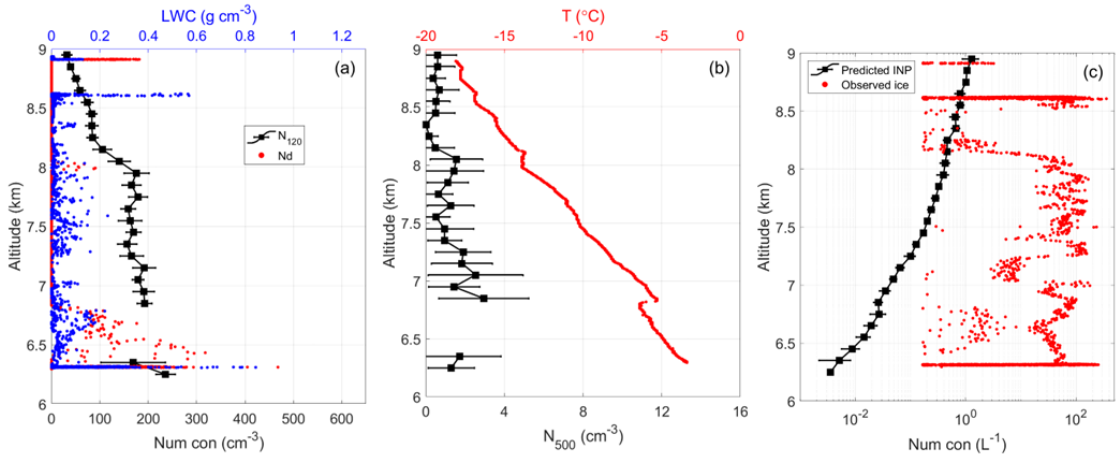

Figure 5: Vertical profiles on 6 July 2014: (a) cloud droplet number concentration from FCDP (N_d, red scatters), LWC from Hotwire (blue scatters) and average aerosol number concentration with size larger than 120 nm (N_{120}, black scatters); (b) temperature (red scatters) and average aerosol number concentration with size larger than 500 nm (N_{500}, black scatters); (c) the concentrations of predicted INP (black line) and observed ice (red scatters).

We have expanded the discussion on the estimation uncertainty of INP concentrations in Sections 2.3 and 4.2.

Lines 135-147:

INP play a crucial role in primary ice formation within clouds, thereby influencing cloud microphysics and precipitation processes (Hoose and Möhler, 2012; Kanji et al., 2017). Recent precipitation-based measurements reported INP concentrations over the TP of 0.002 to 0.675 L^{-1} between −7.1°C and −27.5°C, comparable to those in the Arctic and lower than typical mid-latitude continental values (Chen et al., 2021). Since direct measurements of INP were not available during the TIPEX-III campaign, the empirical parameterization of DeMott et al. (2010) was adopted to infer INP concentrations (N_{INP}). The same scheme has been applied to pristine Antarctic air, where it still performed better than many other available parameterizations, although it was not perfectly applicable (Grosvenor et al., 2012). Accordingly, the N_{INP} (L^{-1}) was estimated from the concentration of aerosols with size larger than 0.5 μm ($N_{a,0.5}$, cm^{-3}) sampled outside clouds:

$$N_{INP} = a(273.16 - T)^b \left(N_{a,0.5}\right)^{c(273.16-T)+d} \quad (1)$$

where T is temperature (K), a = 0.0000594, b = 3.33, c = 0.0264, and d = 0.0033. Therefore, aerosol loading exerts a much weaker influence on N_{INP} than temperature: over the temperature range −2 to −30°C, N_{INP} varies by approximately four orders of magnitude, whereas even a tenfold increase in $N_{a,0.5}$ alters N_{INP} by less than one order of magnitude at any given temperature.

Lines 598-614:

A further source of uncertainty concerns the estimation of INP concentrations. The IMF used in this study relies on the empirical parameterization of DeMott et al. (2010), which was developed from mid-latitude and oceanic data and may not fully represent the unique low-aerosol environment of the TP, especially at low temperatures (Sect. 2.3). Moreover, given that the clean background aerosol concentrations over the TP are substantially lower than those used in the DeMott parameterization development, the estimated INP concentrations are likely overestimated in this study, implying that the reported IMF should be considered as conservative lower bounds of the actual ice enhancement. Additionally, the complex topography of the TP can modulate aerosol vertical transport and spatial distribution (Tan et al., 2021; Zhou et al., 2024), adding further uncertainty to INP estimates. Even if N_{INP} were measured directly, the IMF would remain a diagnostic of ice enhancement rather than a measure of SIP efficiency, because it compares in-cloud ice of both primary and secondary origin with the INP concentrations inferred from aerosol sampled outside cloud, and thus requires that the two describe the same air mass and that no primary ice has been lost since nucleation

(Korolev et al., 2020). Values below unity therefore indicate an inconsistency between the estimate and the observed ice population rather than the absence of SIP, and the ratio cannot be converted into a number of secondary ice crystals per primary INP. Despite these limitations, the observed ice enhancement and its environmental dependences are robust and provide useful constraints for improving microphysical parameterizations in high-altitude cloud models. These findings also highlight the urgent need for in situ INP measurements over the TP, particularly at temperatures below −10°C, to refine SIP efficiency assessments and to develop region-specific INP parameterizations.

(3) limitations of the IMF method

The IMF presents the observed ice concentration relative to the estimated INP concentration (IMF=N_{ice}/N_{INP}). Because the IMF is strongly influenced by temperature, it is used here only as an order-of-magnitude indicator of the contrast between the two concentrations, and is not employed in the subsequent analysis of their dependence on environmental conditions. We have added an explanation in Section 2.3 (Lines 153-156): Since N_{INP} in Eq. (1) is a deterministic function of temperature, the IMF is not independent of temperature, and part of its apparent temperature dependence arises from the denominator rather than from a temperature-dependent SIP efficiency. The IMF is therefore interpreted as the degree to which the ice concentration exceeds the primary-nucleation expectation at a given temperature.

4. Interpretation of Figure 16 may be affected by self-correlation

Section 3.3 relies on the relationships shown in Figure 16 to describe parameters controlling SIP. However, some of these correlations may be partly mathematical rather than physical.

The IMF is defined as

$$\frac{N_{ice}}{N_{INP}} = \frac{N_{irreg} + N_{round}}{N_{INP}}$$

where both irregular and round particle concentrations are components of the numerator.

Figure 16b shows the IMF (SIP ratio) as a function of N_{irreg}. Therefore, N_{irreg} appears on both axes. Likewise, Figure 16a relates SIP ratio to N_{round}, although N_{round} is already contained within the SIP-ratio definition.

As a result, the reported strong correlations may reflect mathematical coupling among the variables rather than independent physical relationships. For a narrow temperature interval, N_{INP} is expected to vary only weakly and can be considered as a scaling coefficient, and much of the apparent relationship may therefore arise from variations in the ratio N_{round}/N_{irreg}. The latter is shown in Fig.16d.

Consequently, the positive correlations between N_{irreg}, N_{round}, and IMF shown in Figure 16 cannot be viewed as independent evidence that drizzle concentration, large droplet concentration, or ice concentration controls SIP intensity.

The authors should either:

- perform an analysis using independent variables,

- quantify the effect of mathematical self-correlation, or
- substantially temper the interpretation of Figure 16.

Without such analysis, Figure 16 provides limited evidence for the proposed SIP mechanisms.

Reply:

(1) The definition of IMF

The manuscript now consistently uses IMF to quantify ice enhancement (Sect. 2.3, IMF=N_{ice}/N_{INP}). Here, N_{ice} is the concentrations of irregular particles (ice) from the 2DS10 and does not include the round (D ≥ 90 μm) concentrations. N_{INP} values were estimated using the parameterization of DeMott et al. (2010).

(2) Redrawing of Fig. 16

Because INP concentrations are highly temperature-dependent, varying by up to two orders of magnitude between −2 and −20°C, the IMF is also strongly influenced by temperature. Therefore, in Section 3.3, we analyzed these variables independently and redrew Fig. 16 to discuss the relationship between ice enhancement and the concentrations of drizzle and large hydrometeors based on all in-cloud samples on 06 July 2014. The samples were averaged over 5 seconds and divided into four groups according to whether the concentrations of drizzle (N_{round}, D ≥ 90 μm) and large hydrometeors (N_{HVPS}, D ≥ 300 μm) reached 1 L^{-1}: Neither, Drizzle only, Large only and Both (Fig. 16). Statistical analysis indicates that strong ice enhancement (N_{ice} > 50 L^{-1}) occurred only where drizzle and large hydrometeors coexisted at all sampled temperatures.

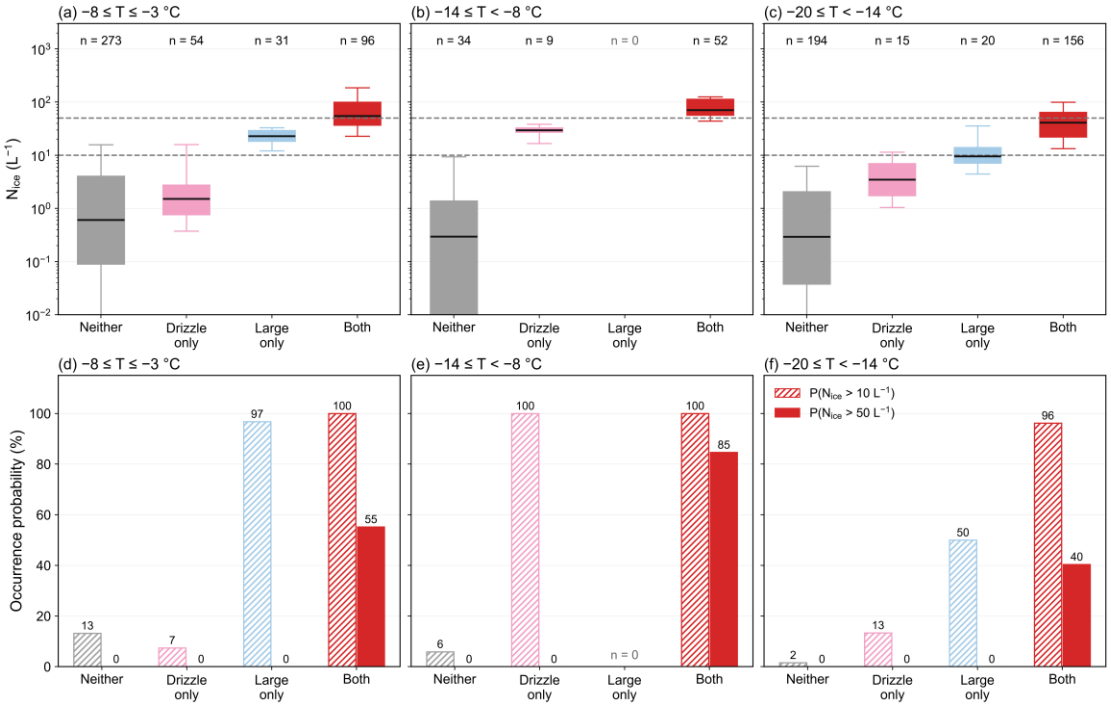

Figure 16: Ice concentrations on 06 July 2014 grouped by the presence of drizzle (Nround (D ≥ 90 μm) ≥ 1 L^{-1}) and large hydrometeors (NHVPS (D ≥ 300 μm) ≥ 1 L–1), based on 5-second averaged in-cloud samples. (a–c) Box plots of Nice for −8 ≤ T ≤ −3°C, −14 ≤ T < −8°C and −20 ≤ T < −14°C; boxes span the interquartile range, whiskers the 5th–95th percentiles, and horizontal lines the medians; dashed lines mark 10 and 50 L–1, and n is the number of samples. (d–f) Occurrence probabilities of Nice > 10 L^{-1} (hatched bars) and Nice > 50

L^{-1} (filled bars) for the same groups and temperature ranges.

5. Identification of drizzle and large drops is highly uncertain

Interpretation of SIP type largely depends on identifying drizzle and large liquid drops using 2DS imagery. Thermodynamic phase classification is primarily based on particle roundness. This approach introduces significant uncertainties. First, 2DS images with 10 µm pixel resolution offer limited shape information for particles smaller than 20 pixels. Compact, non-spherical particles represented by 10–20 pixels can easily appear circular (Korolev et al., 2017). Second, diffraction effects can cause out-of-focus images of compact ice particles to resemble out-of-focus spherical patterns, leading to potential misidentification as liquid drops. Third, a spherical appearance does not necessarily indicate a liquid phase, as frozen drops and compact ice particles may also appear circular. As a result, inferred concentrations of drizzle and large drops may be significantly affected by the presence of ice particles. This issue is especially relevant for Figure 16a, b, and d. Reported drizzle concentrations above 100 L^{-1} at temperatures near −15°C and −20°C (Fig. 16a, d) are unusually high and uncommon at those low temperatures and raise concerns about the phase-classification methodology. Because SIP interpretation depends on identifying drizzle and large drops, the associated classification uncertainty should be quantified.

Reply:

Inspection of the data showed that the anomalously high round concentrations (above 100 L^{-1} near −15°C and −20°C) came from circular particles at the small end of the 2DS10 spectrum, where, as you note, 10-20 pixels image carries very little shape information. Following Taylor et al. (2016), who applied a 50-pixel (about 90 µm) threshold below which no shape classification was attempted, only particles with $D \geq 90$ µm are now assigned to the round (drizzle) or irregular (ice) categories, while smaller circular particles are grouped in a non-phase-discriminated "small" class (Sect. 2.2). For reference, if the full spectrum were used the round concentration would reach about 800 L^{-1}, and about 200 L^{-1} with a 60 µm threshold, both of which are unphysical for supercooled drizzle; with the 90 µm threshold the round concentration is 0 to 50 L^{-1}, which is consistent with in situ drizzle measurements. All figures and statistics involving round concentrations have been recalculated.

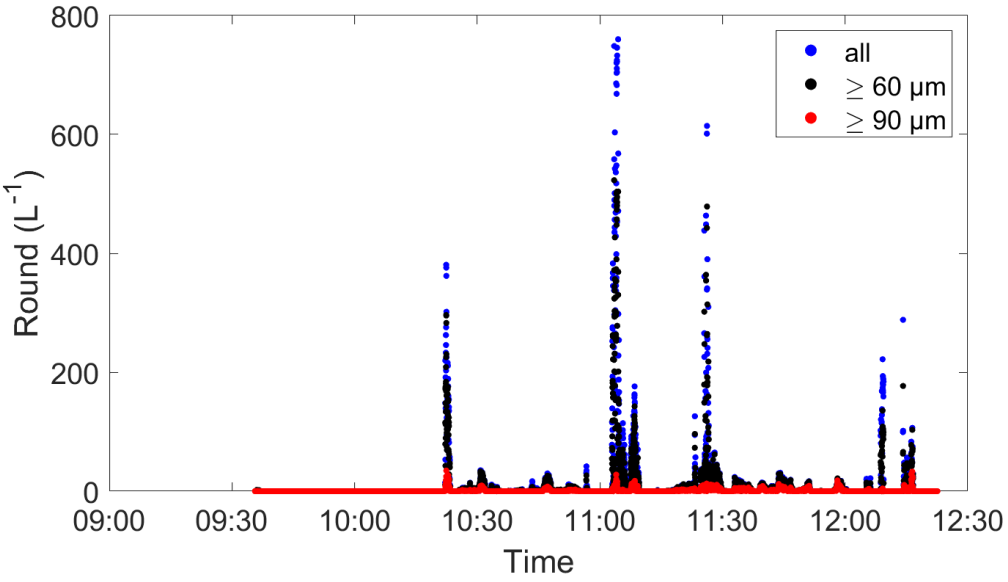

The differences in round concentration were calculated from spectral data using different size thresholds.

We have already explained and clarified this in Sect. 2.2, where the calculation of the round concentration was corrected (Lines 122-127):

For particles smaller than about 90 µm (about 50 pixels), however, shape-based phase discrimination is unreliable and tends to inflate the apparent round (liquid) concentration. Adopting the same practice as Taylor et al. (2016), shape classification was performed on all particles, but the 90 µm threshold was applied to the round class only. Particles with $0.9 \leq C < 1.2$ and $D \geq 90$ µm were therefore classified as round particles (drizzle), whereas smaller circular particles were grouped into a non-phase-discriminated "small" category. In addition, images with $C \geq 1.2$ were classified as irregular particles (ice).

6. Evidence for freezing droplet fragmentation is inconclusive

The manuscript interprets CPI images presented in Figure 9 as evidence for frozen-drop fragments produced by active droplet shattering. Visual inspection of the images does not reveal clear examples of characteristic frozen-drop fragments. Previous studies have typically relied on identifiable fragmentation products to infer active freezing droplet breakup SIP mechanism. The evidence presented in Figure 9 is insufficient to support the conclusion that freezing droplet fragmentation was active; thus, this interpretation remains speculative. The discussion should be significantly toned down.

Reply: We have reselected the CPI images for Fig. 9. Unfortunately, because a considerable amount of CPI image data is missing, no images that effectively support the DS mechanism have been found so far. Therefore, in this manuscript, we can only make reasonable inferences and discussion regarding the existence of the DS at different temperatures based on temperature, ice concentrations, round concentrations, and some CPI images. The discussion of the DS mechanism in the text has also been weakened.

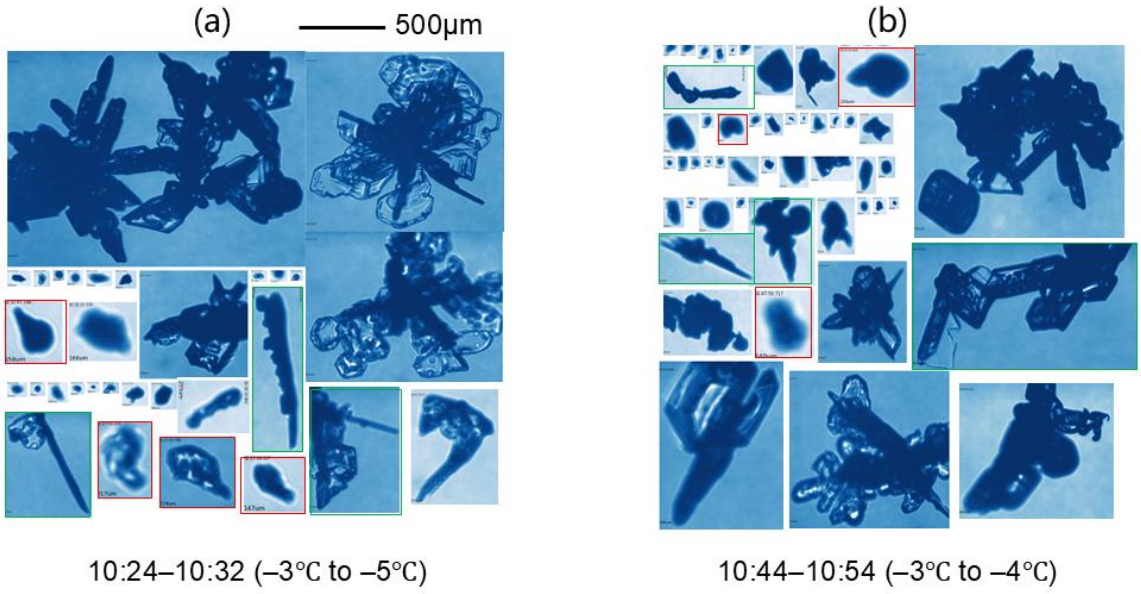

Figure 9: Example CPI images of panel (a) case 1 and panel (b) case 2.

7. Attribution to collisional breakup is speculative

The evidence supporting the collisional-breakup mechanism is even less convincing. Currently, no observational technique can determine whether a fragmented ice particle sampled by an airborne probe originated from collisional breakup in the cloud or from shattering upon interaction with the probe itself. Therefore, attributing enhanced ice concentrations to active collisional breakup remains speculative. While this mechanism cannot be excluded, the presented observations do not provide direct evidence that it occurred.

Reply:

As with the DS inference, the current observational data do not provide direct evidence for the occurrence of BR. We can only infer from dendritic snowflakes and their fractured dendritic structures that a BR process may have occurred and thus caused the ice enhancement. The discussions of DS and BR in the text have been revised accordingly (Lines 286–301):

In addition to the HM process, the CPI images in Fig. 9 further exhibit particle features that are morphologically consistent with other possible SIP mechanisms. Dendritic snowflakes were clearly present in cases 1 and 2, and were inferred to have formed at higher (colder) levels and to have sedimented into this layer. The CPI images highlighted by green boxes show broken branches and detached fragments adjacent to fragile dendritic snowflakes, features that are morphologically consistent with BR. Collisional breakup of ice particles near –5°C has been documented to produce fine needles and columnar fragments (Hou et al., 2023; Knight, 2012). Korolev and Leisner (2020) also noted that BR is most likely in mixed-phase convective regions. Therefore, these fragments in Fig. 9 could potentially originate from the collisional breakup of dendritic snowflakes. However, no observational technique can determine whether such fragments originated from the BR process within the cloud or from shattering upon interaction with the probe itself, and similar detachments may also arise from other mechanical processes. Furthermore, the supercooled droplets in Fig. 9 marked by red

boxes have small fragments in their immediate vicinity, a morphology that could result from the freezing and subsequent fragmentation of droplets. Identifiable fragmentation products of the type used in previous studies (Lawson et al., 2015, 2017; Korolev et al., 2020) to infer active droplet shattering are not clearly evident in these images, and comparable morphologies may also arise from other processes such as HM or probe shattering. Overall, the present interpretation is based solely on limited CPI images and carries considerable uncertainty, but we cannot rule out contributions from SIP mechanisms other than HM to the ice enhancement observed in cases 1 and 2.

8. Several conclusions overstate novelty and significance

Several conclusions need revision.

Conclusions 2 and 3 largely repeat results that have been reported in previous SIP studies and should be discussed in the context of the broader literature.

The statement:

"… our results demonstrate that the effective SIP temperature range over the TP extends to −16°C through the coexistence of HM, DS, and BR mechanisms, with the SIP ratio reaching up to 1000, substantially higher than the enhancement factors in other regions"

is not supported for several reasons:

1. The coexistence of HM, DS, and BR mechanisms has not been demonstrated. On top of that, the coexistence of these mechanisms was discussed in previous observational and modeling studies.

2. Enhanced ice concentrations observed at −16°C do not imply locally active SIP at −16°C.

3. Observations of SIP with IMF values exceeding 1000 have already been reported by Ladino et al. (2017), Yang et al. (2020), Järvinen et al. (2022), and Wieder et al. (2022).

Therefore, neither the mechanism attribution nor the claimed uniqueness of the observed SIP ratios (IMF) is justified.

Reply:

We agree with each of the three points, and the Conclusions have been rewritten accordingly.

(1) The previous version stated that HM, DS and BR coexist and divide the temperature range between them. That statement has been removed. The manuscript no longer identifies specific SIP mechanisms; it presents the observational evidence consistent with ice enhancement and states which processes could contribute without assigning a role to any of them. DS and BR are now mentioned only as processes whose contribution the observations cannot exclude.

(2) We agree that enhanced ice concentrations at −16°C do not imply locally active SIP at −16°C. Section 3.2.2 now discusses the vertical transport of ice formed at warmer levels, supported by the ERA5 vertical velocity fields in Fig. 15, and the cold-level enhancement is presented as arising from transport, from local SIP, or from both. The claim that the effective SIP temperature range extends to −16°C has been deleted; the text now states that the enhancement persisted to −16°C.

(3) The IMF value is a result of this study and is reported as such: the maximum ice concentrations reached 253.6 L^{-1} and the IMF exceeded 10000 near −4°C (N_{INP} below 0.01 L^{-1}). What we accept is that the value does not constitute a new record. The statement that it was substantially higher than the enhancement factors in other regions has been deleted, and Table 3 now places it within the range already reported (Ladino et al., 2017; Yang et al., 2020; Järvinen et al., 2022). The interest of the TP case lies in the environment in which such values were reached, a clean aerosol background with persistent supercooled liquid water, rather than in the magnitude itself.

9. Insufficient meteorological context

Although the manuscript states that the observations were collected within a mesoscale convective cloud system, the meteorological context is not adequately described. Important missing information includes: cloud-top altitude, cloud-base altitude, melting-layer altitude, cloud-top temperature, cloud-base temperature, cloud lifetime, storm evolutionary stage (developing, mature, decaying). This information is essential for interpreting cloud microphysics and may be obtained from radar and satellite observations.

Reply:

Fig. 2 has been extended and Sect. 3.1 rewritten. Fig. 2 now shows the FY-2D visible image, TBB, the composite reflectivity from the Naqu C-band radar and the Naqu sounding. In addition, the ground-based radar reflectivity profile has been plotted on the time series figure for each case, which can serve as a reference for the development stage of the cloud system. The meteorological background is described in manuscript as follows (Lines 180–192):

Figure 2 shows the meteorological background on 06 July 2014. FY-2D visible-band cloud image presents vigorous convection over the TP with mesoscale convective cloud clusters in the aircraft observation region characterized by bright white cloud tops and deep vertical development (Fig. 2a). In the region where the aircraft operated, the FY-2D brightness temperature was lower than −20°C, indicating cold cloud tops and reaching −30 to −40°C over the convective cores (Fig. 2b). The composite radar reflectivity from the Naqu radar further reveals that the aircraft penetrated the core region of the convective systems and performed multiple sampling passes near the strong echo center, with core reflectivity exceeding 30 dBZ (Fig. 2c). The Naqu sounding places the 0°C level at approximately 5854 m, with the −10°C and −20°C levels at about 7830 and 9411 m, respectively (Fig. 2d). Southwesterly winds prevailed between 6 and 9 km and veered to westerly above 9 km. The lifting condensation level (LCL) was 4685 m and the convective condensation level (CCL) was 5043 m. Consequently, the cloud base was estimated at 4.7–5.0 km, which lies 0.8–1.2 km below the 0°C level and thus well within the warm layer. This configuration results in an in-cloud warm layer approximately 1 km deep between the cloud base and the 0°C level, within which collision-coalescence can produce drizzle-sized drops that updrafts may subsequently carry above the 0°C level as supercooled large droplets.

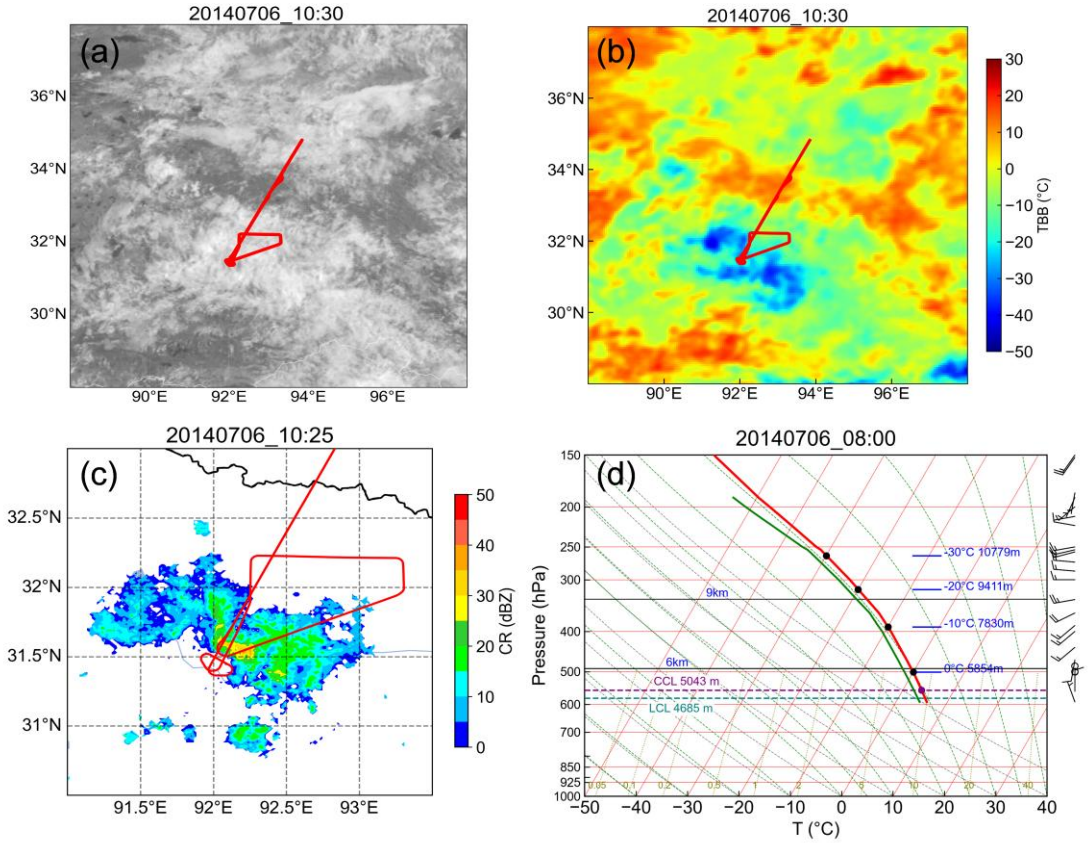

Figure 2: (a) satellite FY-2D visible-band cloud image at 10:30, (b) brightness temperature at 10:30, (c) composite radar reflectivity from the C-band ground-based Naqu radar at 10:25 and (d) Naqu sounding profile at 08:00 (red line is temperature, and green line is dew point temperature). The red line in (a)–(c) denotes the aircraft track on 06 July 2014.

10. Exclusion of HVPS measurements

It is unclear why HVPS observations were not incorporated into the particle size distributions shown in Figures 10 and 15. Because the largest hydrometeors often play an important role in SIP-related processes, omission of HVPS measurements results in incomplete characterization of particle size spectra. The authors should either include the HVPS measurements or clearly justify their exclusion.

Reply:

HVPS spectra have been added to Figs. 10 and 14 (original 15). For each case the figure now shows the mean spectrum of irregular particles from 2DS, of round particles from 2DS ($D \geq 90$ μm), and of all particles from HVPS, so that the ice, drizzle and large hydrometeors can be followed from μm-size to the mm-size range in clouds.

Three results as follows:

(1) In SIP-active legs, bimodal ice spectra (modes below 100 μm and at 200–300 μm) coincided with drizzle and large hydrometeors,

(2) The presence of large hydrometeors (such as graupel and large snowflakes) provides favorable conditions for SIP, as they act as indispensable collision partners or riming substrates.

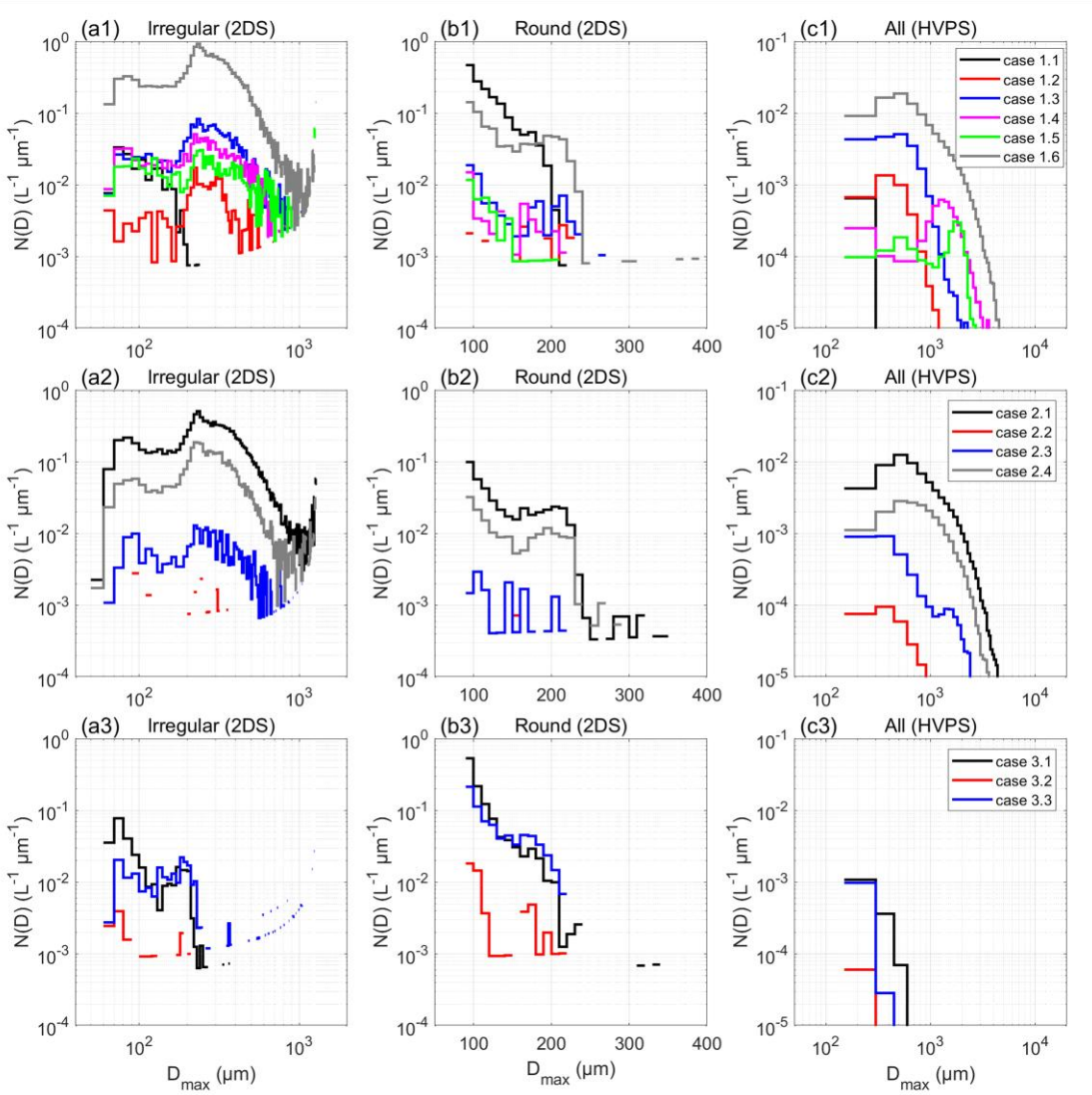

Figure 10: Mean size distributions (step plots) of (a1–a3) irregular particles from 2DS, (b1–b3) round droplets from 2DS, and (c1–c3) all particles from HVPS for cases 1–3. Different coloured lines represent selected legs within each case.

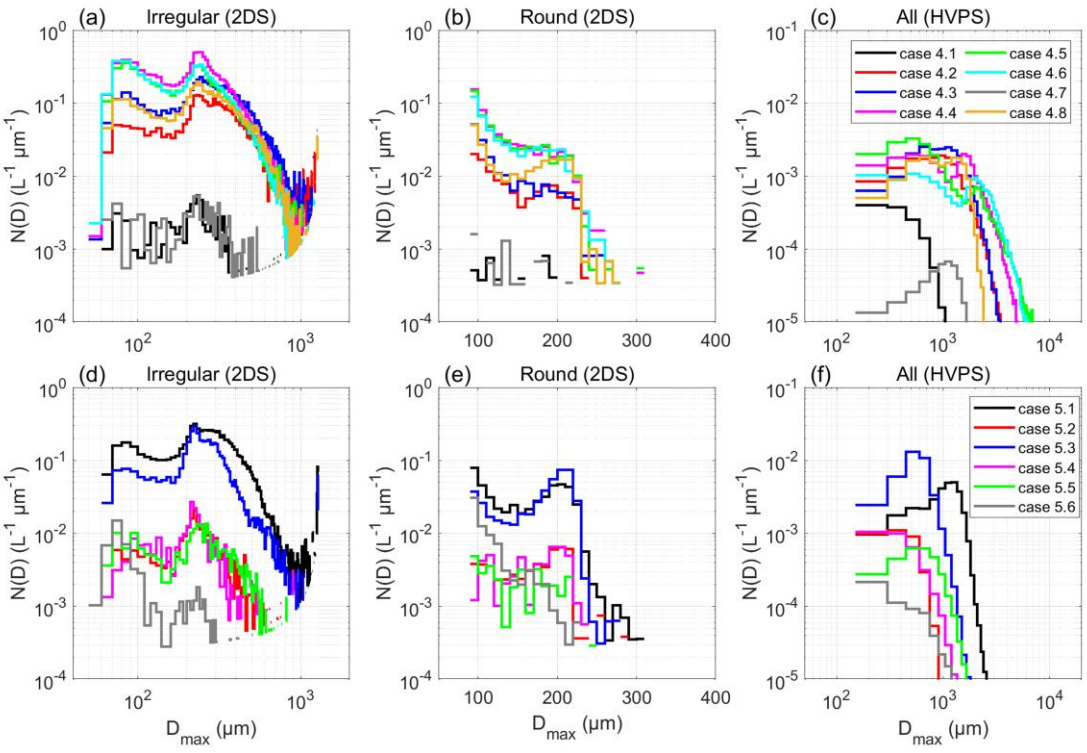

Figure 14: Mean size distributions (step plots) of ice particles (left), droplets (center) from 2DS and all particles(right) from HVPS: (a, b, c) case 4 and (d, e, f) case 5. Different coloured lines represent selected legs within each case.

11. Literature review is incomplete

Over the last several decades, numerous in situ and remote-sensing studies have documented SIP events in a variety of cloud systems and climatic regions.

Table 2 contains only a limited subset of these observations and appears strongly biased toward Northern Hemisphere studies. To place the present work into a broader context, I recommend a substantially more comprehensive review of previous SIP observations and expansion of Table 2.

Reply:

Table 3 has been rebuilt and now covers the Northern Hemisphere (Tibetan Plateau, other regions of China, South Asia, the Arctic, North America, Europe, Alpine orographic clouds), the Southern Hemisphere (Southern Ocean and Australia, Antarctic Peninsula and coast) and the tropics (convective and stratiform clouds), with the temperature range, the SIP signature and the reported ice enhancement for each entry.

Sect. 4.1 has been expanded accordingly and draws three conclusions from the comparison: that most reported enhancements fall within, or only slightly beyond, the classical HM window; that the coexistence of columnar or needle crystals, graupel and supercooled droplets within that window is almost universal; and that the mechanistic attribution becomes progressively less certain at colder temperatures. The section also compares the magnitude of the enhancement across regions and concludes that the absolute ice concentration is controlled more by cloud type and dynamics than by geographical region, with the TP values falling within the range reported for mid-latitude and tropical convection.

Table 3: Overview of field observations of SIP across regions (Currently, the specific mechanisms of SIP in all observations are only hypothesized possible mechanisms, not definitive mechanism attributions. Ice concentration values in different regions may also differ due to differences in calculation methods and instruments).

Hemisphere	Region	Temperature	SIP signature	Reported ice enhancement
Northern Hemisphere	TP convective clouds from aircraft TIPEX-III (Zhao et al., 2023; this study)	−3 to −8°C (Zhao et al., 2023); −3.6 to −16.3°C (this study)	−3 to −8°C: HM process appears to be the dominant SIP mechanism (Zhao et al., 2023); columnar crystals, graupel and large droplets observed (Zhao et al., 2023; this study); T<−8°C: ice enhancement consistent with the upward transport of secondary ice formed at warmer levels, although it cannot be separated from local SIP (this study).	Max Nice: 285 L^{-1} (Zhao et al., 2023), 253.6 L^{-1} (this study); the IMF can exceed 10000 near −4°C (this study).
	Other regions in China, aircraft in situ (Yang et al., 2014, 2017; Zhao and Lei, 2014; Hou et al., 2021, 2023; Wang et al., 2023; Li et al., 2024; Du et al., 2024; Long et al., 2025)	−3 to −17°C	−3 to −8°C: HM-consistent signatures, columnar/needle crystals, graupel and large supercooled droplets observed (Yang et al., 2014, 2017; Zhao and Lei, 2014; Hou et al., 2021, 2023; Li et al., 2024; Long et al., 2025); at colder temperatures: DS inferred in stratiform clouds of eastern China (Wang et al., 2023), and BR consistent with dendrite fragmentation (Zhao and Lei, 2014); seeder-feeder interaction extends SIP to about −14°C (Du et al., 2024).	Max Nice: up to about 300 L^{-1} (Yang et al., 2017; Wang et al., 2023; Du et al., 2024), often exceeding parameterized N_{INP} by one to three orders of magnitude; no unified IMF reported.
	South Asia aircraft in situ (Patade et al., 2016; Kambrath et al., 2024)	−3 to −8°C	HM, with coexisting small and large droplets, rimed needles and columns, and snow particles (or graupel)	Max Nice (>100 μm): 300 L^{-1}, more than INP (mean 5 L^{-1}, Patade et al., 2016); up to 1000 L^{-1} (Kambrath et al., 2024)
	Arctic mixed-phase Aircraft in situ (Rangno and Hobbs, 2001; Pasquier et al., 2022; Korolev and Lawson, 2026); remote sensing (Luke et al., 2021)	−3 to −24°C	−3 to −5°C: DS, down to −24°C: BR (Pasquier et al., 2022); −2.5 to −8°C: HM may partly rely on high ice concentrations; T< −8°C: BR and DS (Rangno and Hobbs, 2001); T>−10°C: DS inferred as the more efficient mechanism than HM (Luke et al., 2021)	Max Nice: up to 150 L^{-1} (Pasquier et al., 2022); Nice >5 orders of magnitude above measured N_{INP}, but SIP-favorable conditions were seldom present (Korolev and Lawson, 2026); 1000-fold ice enhancement (Luke et al., 2021)
	North America aircraft in situ (Lawson et al., 2017; Korolev et al., 2020, 2022;	0 to −27°C	DS was proposed as a new SIP process by Lawson et al. (2017) from freezing of mm-sized supercooled	Nice exceeding N_{INP} by up to about 4 orders of magnitude (Korolev et al., 2020); 5–8 fragments per freezing

Hemisphere	Region	Temperature	SIP signature	Reported ice enhancement
	Lachapelle et al., 2025; Biggart et al., 2026)		drops (−8 to −18°C), and is clearly supported by in-situ observations from 0 to −15°C (Korolev et al., 2020); down to −27°C: DS and BR may be plausible SIP mechanisms (Korolev et al., 2022); DS during freezing-rain precipitation with bimodal PSDs (Lachapelle et al., 2025); CAO cloud from −3 to −8°C: HM; −15 to −18°C: BR (Biggart et al., 2026)	drop, about 500 L^{-1} small ice (Lachapelle et al., 2025); Nice peak excess about 4 orders over INP in the HM region (Biggart et al., 2026)
	Europe aircraft in situ (Crosier et al., 2011, 2014; Huang et al., 2008, 2011; Crawford et al., 2012; Taylor et al., 2016; Jackson et al., 2018); ground-based in situ and remote sensing (Pfeifer et al., 2025)	−3 to −14°C; 0 to −3°C for refreezing rain (Pfeifer et al., 2025)	−3 to −10°C: HM (Crosier et al., 2011, near −5°C; Huang et al., 2008, 2011; Crawford et al., 2012; Crosier et al., 2014; Taylor et al., 2016; Jackson et al., 2018); −12 to −14 °C: DS (Jackson et al., 2018); DS during refreezing rain process (Pfeifer et al., 2025)	Max Nice: 70–400 L^{-1} (aircraft in situ); 1.2–6.1 fragments per freezing drop (ground-based in situ and remote sensing)
	Alpine orographic, ground-based remote sensing with tethered-balloon in situ (Ramelli et al., 2021; Lauber et al., 2021)	About −3°C (Ramelli et al., 2021); 0 to −3°C (Lauber et al., 2021)	HM and BR likely in the low-level feeder cloud (Ramelli et al., 2021); 0 to −3 °C: DS, with drizzle drops of ~200 µm (Lauber et al., 2021)	Max Nice: 14 L^{-1}, with Nice (<100 µm) of 1–2 L^{-1}, about 3 orders of magnitude above N_{INP} (Ramelli et al., 2021); 18 secondary ice crystals per 200 µm freezing drop (Lauber et al., 2021)
Southern Hemisphere	Southern Ocean and Australia, aircraft in situ (Mossop, 1985; Järvinen et al., 2022; Huang et al., 2017, 2021; Lasher-Trapp et al., 2021; Finlon et al., 2020)	−3 to −12°C	−3 to −8°C: HM, supported by columnar crystals (Mossop, 1985; Finlon et al., 2020; Järvinen et al., 2022; Huang et al., 2017, 2021); cold-layer SIP mechanism (may be BR and/or DS) unresolved (Järvinen et al., 2022; Huang et al., 2021); HM favored in multi-updraft cumuli, which retain frozen drops and graupel in the HM zone for longer (Lasher-Trapp et al., 2021);	Max Nice: 54–205 L^{-1} (Mossop, 1985; Huang et al., 2017, 2021; Finlon et al., 2020; Järvinen et al., 2022); Nice up to 7 orders of magnitude above N_{INP} (Lasher-Trapp et al., 2021)
	Antarctic Peninsula and coast aircraft in situ (Grosvenor et al., 2012; Lachlan-Cope et al., 2016; O'Shea et al., 2017)	−3 to −8°C	HM with columnar and rimed crystals (Grosvenor et al., 2012; O'Shea et al., 2017); secondary ice multiplication (likely HM) peaking at around −5°C (Lachlan-Cope et al., 2016)	Nice up to 7 L^{-1} in the HM layer against background ice (<0.1 L^{-1}) (Grosvenor et al., 2012); 1–3 orders of magnitude above N_{INP} (O'Shea et al., 2017); east Nice about 0.74 L^{-1},

Hemisphere	Region	Temperature	SIP signature	Reported ice enhancement
				west about 1.73 L^{-1} (Lachlan-Cope et al., 2016)
Tropical	Tropical aircraft in situ: Convective clouds (Heymsfield and Willis, 2014; Lawson et al., 2015; Lasher-Trapp et al., 2016; Ladino et al., 2017; Lloyd et al., 2020; Korolev et al., 2024); Stratiform mixed-phase clouds (Yang et al., 2020)	0 to −20°C	**Convective clouds:** Weak (±1 m s^{-1}) updrafts and low LWC (<0.1 g m^{-3}) favorable for SIP (Heymsfield and Willis, 2014); −12 to −20°C: DS strongly supported by observations (Lawson et al., 2015); −3 to −8°C: HM favored, with graupel recirculating through the HM zone (Lasher-Trapp et al., 2016); −5 to −14°C: HM and DS cannot be separated, and high concentrations of potential secondary ice occur even where graupel is absent (Ladino et al., 2017); 0 to −5°C: ice present at temperatures too warm for dust INP, morphology consistent with DS, primary and secondary ice not separable (Lloyd et al., 2020); −2 to −5°C: DS combined with recirculation of drops through the melting layer (Korolev et al., 2024) **Stratiform mixed-phase clouds:** −5 to −8°C: needles and columns with drizzle drops (>100 μm) but no significant riming, so primary nucleation, HM and DS are all insufficient (Yang et al., 2020)	**Convective cloud:** Max Nice: 100–572 L^{-1} (Heymsfield and Willis, 2014; Lawson et al., 2015; Lasher-Trapp et al., 2016; Lloyd et al., 2020); even up to 1000 L^{-1} (Korolev et al., 2024) **Stratiform mixed-phase clouds:** Max Nice 0.05–5 L^{-1}, up to 10 L^{-1} including an adjacent pileus cloud (Yang et al., 2020)